Massó Ramírez, A.; Ivars-Barceló, F.; López Nieto, JM. (2020). Optimizing Reflux Synthesis Method of Mo-V-Te-Nb mixed oxide Catalysts for Light Alkane Selective Oxidation. Catalysis Today. 356:322-329. https://doi.org/10.1016/j.cattod.2019.10.030

Optimizing Reflux Synthesis Method of Mo-V-Te-Nb mixed oxide Catalysts for Light Alkane Selective Oxidation

by

Amada Massó Ramírez [a], Francisco Ivars-Barceló [b,*], José M. López Nieto [a,*]

[a] *Instituto de Tecnología Química, Universitat Politècnica de València-Consejo Superior de Investigaciones Científicas, Avenida de los Naranjos s/n, 46022 Valencia, Spain.*

[b] *Dpto. de Química Inorgánica y Química Técnica, Facultad de Ciencias de la Universidad Nacional de Educación a Distancia (UNED), Paseo Senda del Rey 9, 28040 Madrid, Spain.*

* *E-mail: jmlopez@itq.upv.es; franciscoivars@ccia.uned.es*

Abstract

The investigation here presented studies the effect of the synthesis temperature (from 80 to 110 °C) and the time (from 1 to 4 days) employed to precipitate catalyst precursors by reflux method, on the physic-chemical and the catalytic properties of the resulting Mo-V-Te-Nb mixed oxide catalysts for both propane partial oxidation into acrylic acid and ethane oxidative dehydrogenation (ODH) to ethylene. The insight obtained has allowed an important optimization of the not commonly used reflux method to prepare Mo-V-Te-Nb oxide materials with competitive catalytic performance. The yields achieved overcome those from optimized catalysts prepared by conventional hydrothermal method, and approach those reached with catalysts prepared using the "slurry method". The optimum rise for the synthesis temperature is found as a key factor for the reflux method. It allows access to an increased vanadium content into the reflux precipitate, which favors the formation of a pseudo-amorphous Mo-V-Te-Nb oxometallate. This precipitate behaves as a precursor for the crystallization, during the solid-state activation step at high-temperature (600 °C/N_2), of the structure type $(TeO)_2M_{20}O_{56}$ (*M*= Mo, V, Nb), key for the selective conversion of propane. On the other hand, for the optimum temperature of synthesis, i.e. 110 °C, higher synthesis time of the precursor leads to smaller crystal sizes in the final catalyst (higher specific surface areas) and lowers the average oxidation state of vanadium from V^{+5} to V^{+4}, which significantly enhances the catalytic behavior.

Keywords: light alkanes, oxidation, propane, acrylic acid, ethane, ethylene, oxidative dehydrogenation, ODH, Mo-V-Te-Nb oxides, reflux, M1 phase.

1. Introducción

Mixed metal oxides are important catalysts in partial oxidation of hydrocarbons [1-6]. One of the more important catalytic systems developed in the last two decades is the Mo-V-Te-Nb mixed oxide system, effective catalysts for light hydrocarbons partial oxidation reactions [1-7]. Especially relevant are their properties for the selective (amm)oxidation of propane into acrylic acid or acrylonitrile [8-10] and the oxidative dehydrogenation of ethane to ethylene [11, 12], both reactions addressed to substitute the corresponding industrial processes based on olefins currently established [13-15]. The use of alkane natural resources as raw materials, such as propane or ethane (present in LPG and NG), instead of olefins (produced in high energy-consuming processes), intrinsically links to a more sustainable technology [13, 15].

The preparation of the Mo-V-Te-Nb based catalysts takes place in two separated stages: 1) synthesis of the solid precursor, and 2) precursor solid-state activation at high temperature. The so-called "slurry" [8-10, 16-21] and "hydrothermal" methods have been commonly employed for the synthesis of the solid precursors. Also, spray-drying was proposed for preparing catalyst precursors [22-24]. However, a final activation of catalysts, a heat-treatment at *ca.* 600ºC in an inert atmosphere, is needed for preparing the actual catalysts [25, 26]. Additionally, a post-synthesis purification step can improve the catalytic behavior of these catalysts [27]. Important changes in catalytic performance and the nature of crystalline phases have been observed depending on the catalyst preparation methods and/or the starting materials [8-10, 16-27]. In addition, small changes in the physic-chemical characteristics of catalysts can be observed during the reaction [28]. Nevertheless, the use of the aforementioned synthesis methods has not brought significant improvements to the catalytic performance of Mo-V-Te-Nb mixed oxide systems since the first works published in the '90s [8-10].

Despite their advantages, those traditional methods present restrictions that could be limiting the development of materials with enhanced catalytic properties. Several years ago, it was proposed the reflux synthesis as a promising alternative method to overcome conventional methods restrictions [29]. With the reflux method, the desired atmosphere can be established for the synthesis at temperatures above the boiling point of the solvent (a feature shared by the hydrothermal method). Solvent loss by evaporation is prevented, so the synthesis conditions and parameters depending on the solvent volume are always under control. Moreover, it is possible to interact with the system at all times, monitoring and tracking synthesis parameters (a feature shared by the slurry method). However, the so far reported catalysts prepared by reflux require very long synthesis times (14 days) and yet present not very competitive catalytic performance for propane selective oxidation to acrylic acid [29].

Against this backdrop, a systematic study on the effect of key parameters for the synthesis of Mo-V-Te-Nb oxides by reflux method, such as temperature and time of reflux to obtain the precursor, is conducted in this work. The successful optimization of the corresponding catalytic properties for the selective oxidative transformation of propane and ethane, together with a drastic reduction of the synthesis times are presented as a result.

2. Materials and Methods

2.1. Preparation of metal oxides catalysts

Solid catalyst precursors were prepared by reflux at different temperatures (80, 100 or 110 °C) and synthesis times (1, 2 or 4 days), starting from aqueous solutions mixtures of $(NH_4)_6Mo_7O_{24}\cdot 4H_2O$ (Merck), NH_4VO_3 (Aldrich), $Te(OH)_6$ (Aldrich), and $(NH_4)_2Nb_2(C_2O_4)_5$ (CBMM), keeping a constant molar ratio Mo/V/Te/Nb of

1.00/0.30/0.16/0.16 in the synthesis gel. The resulting precipitates were filtrated and washed with distilled water, and finally dried in air at 100 °C for 12 h. Dried solids (precursors) were thermally activated at 600 °C for 2h, in a N_2 stream (15 ml min^{-1} flow), giving rise to the final catalysts. The precursors have been named as L-t, M-t and P-t were L, M and P correspond to samples prepared at the reflux temperature of 80, 100 and 110ºC, respectively; and "t" refers to the synthesis time (in days). The final catalysts, after the thermal activation treatment above described, have been named with an "A" at the end of the name used for their corresponding precursors.

2.2. Characterization of solids

The chemical analysis of the solids has been performed by inductively coupled plasma atomic emission spectrometry (ICP-AES).

The specific surface areas have been determined by the BET method from N_2 adsorption isotherms at 77 K measured in a *Micromeritics TriStar 3000* instrument. A desorption treatment at 400ºC (heating rate of 10 ºC min^{-1}) for 1h under a high vacuum range was conducted for every sample just prior to the BET analysis.

X-ray diffraction (XRD) patterns of powder solids were collected with a *PANalytical CUBIX* instrument equipped with a graphite monochromator, employing Cu Kα radiation (λ=0.1542 mm) and operated at 45 kV and 4 mA. Distribution of crystalline phases forming the catalysts was calculated by *Rietveld* refinement of the XRD patterns employing *X´Pert Highscore Plus* software.

Solids imagery by field emission scanning electron microscopy (FESEM) was performed using a *JEOL JSM 6300 LINK ISIS* instrument, equipped with an energy dispersive X-ray

analyzer with which chemical composition microanalyses of selected areas were implemented.

UV-vis diffuse reflectance spectroscopy measurements of the solids were carried out within the 200-800 nm range using a *Varian* spectrometer model Cary 5000.

Temperature programmed reduction (TPR) experiments were performed using a *Micromeritics Autochem 2910* instrument. The analyses were carried out with 50 ml min^{-1} total flow of a H_2/He mixture (5% H_2) on 50 mg of catalyst, within the 100–700 ºC temperature range (heating rate of 10 ºC min^{-1}) and employing a thermal conductivity detector (TCD). A pre-treatment flowing Ar (50 ml min^{-1}) for 30 min was conducted for every sample.

Photoelectron spectra (XPS) were recorded on a SPECS spectrometer with a 150 MCD-9 detector and using a nonmonochromatic Al Kα (1486.6 eV) X-ray source. Spectra were recorded using an analyzer pass energy of 30 V, an X-ray power of 100 W, and operating pressure of 5×10^{-10} Torr. Spectral treatment was performed using the CASA software. Binding energies (BE) were referenced to the C 1s peak at 284.5 eV.

2.3. Catalytic Studies

A fixed-bed tubular quartz reactor was utilized to study the catalytic properties of the different Mo-V-Te-Nb oxide catalysts [11, 19]. The catalytic tests in both the partial oxidation of propane and the oxidative dehydrogenation of ethane were performed within the temperature range of 340-440 °C. A particle size range of 0.3-0.5 mm was established for the catalysts during the catalytic tests, the mass of which was varied to obtain catalytic results at different contact times. The reaction feed consisted of a mixture of $C_3H_8/O_2/H_2O$/He (propane oxidation) or C_2H_6/O_2/He (for ethane ODH) with a molar ratio

of 4/8/30/58 or 9/7/84, respectively, employing a total flow of 50 ml min^{-1} [11, 19, 38]. Reactants and products were analyzed online employing a gas chromatograph equipped with two columns (3m length Molecular Sieve 5Å; and 3m length Porapak Q) and a TCD detector. As the amount of sample employed largely varies depending on the experiment, the catalysts have been diluted with silicon carbide to keep a constant volume for the catalytic bed. Blank reaction experiments with no catalyst in the reactor tube showed no conversion within the reaction temperature range 340-440 °C tested. In all cases, carbon balances were 100 ± 4%, irrespective of the catalyst type and mass used.

3. Results and Discussion

3.1. Study of Catalyst Precursors

Powder XRD patterns of the precipitates obtained by reflux at different temperatures (80, 100 or 110 °C) and synthesis times (1, 2 or 4 days) appear very similar among them (Figure 1), with broad and low-intensity peaks indicative of solids with short-range periodic order. All XRD patterns display bands centered at 2θ angles of 22 and 28 °, which appear as main diffractions in some molybdates with perovskite-type derived structure [23, 30]. Concretely, similar XRD patterns have been reported for $Mo_{3.5}VW_{0.5}O_{14}$, which was called a semi-crystalline Mo–V based oxide [23]. By HR-TEM investigations, H. Hibst and co-workers characterized the Mo_5O_{14}-type derived phase $Mo_{3.5}VW_{0.5}O_{14}$ as an intergrowth of different oxidic bronze structures with different channel sizes and without any long-range order in the *a* and *b* planes [23]. The authors described the structural motifs as an analog to another real structure based on ReO_3-blocks intergrowths with corner-shared NbO_6 octahedra, showing different block sizes and no long-range order in *a* and *b* planes. Despite the similitude in the position of the diffraction bands between

$Mo_{3.5}VW_{0.5}O_{14}$ structure and our reflux precipitates, the former present a higher relative intensity for 22 ° 2θ peak, and the presence of resolved peaks within the band from 40 to 60 ° 2θ. Diffraction peak at 2θ = 22 ° corresponds to the typical 4Å distance between consecutive [001] planes of Mo cations in oxygen octahedral coordination [17].

In general, no important difference is appreciated among the diffraction patterns of precipitates as a function of temperature and/or time of reflux synthesis. Nevertheless, the presence of a small low angle peak (2θ = 8 °) seems to be slightly favored at increasing synthesis times and lower temperatures. This low angle peak has been observed in Keggin-type structure polyoxomolybdates with NH_4^+, H^+ and/or K^+ compensation cations [31-33]. The diffraction peak at 2θ= 28° has been also observed in polyoxometalate structures [34]. Regardless of the above, no conclusive statement can be done on the accurate structure/s present in the reflux precipitates from XRD results.

Notwithstanding the XRD similarities among all reflux precipitates obtained, significant differences are observed in their chemical composition (Table 1) as a function of synthesis time and especially of reflux temperature. Thus, the maximum variation is observed when comparing V/Mo and Te/Mo molar ratios between precipitates obtained at the lowest and highest temperature, i.e. at 80 and 110 °C. With respect to the changes in V and Te contents as a function of time, they are especially relevant at 80 °C, gradually becoming less significant as increasing the reflux temperature. In general, variations in the Nb/Mo molar ratio are less significant.

For the reflux precipitates prepared at 80 °C, the content in both V and Te appears favored with the synthesis time, while the Nb slightly decreases. Concretely, the V/Mo molar ratio in the reflux precipitates is almost doubled (from 0.6 to 0.11) and that of Te/Mo increased more than 30% (from 0.16 to 0.21) as going from 24 to 96 h of synthesis at 80 °C.

Contrarily, the Nb/Mo molar ratio decreases *ca.* 20 % from 24 to 48 h remaining relatively constant at higher synthesis time.

The incorporation of either V or Te in the reflux precipitate appears favored as increasing the reflux temperature as well, although the dependence with the synthesis time at the set temperature is gradually vanishing. Thus, in contrast with the precipitates at 80 °C, extending the synthesis times at 110 °C induced no significant correlation nor variation of V/Mo or Te/Mo molar ratios in the resulting precipitate (Table 1). Nevertheless, moving from 80 to 110 °C for the same synthesis time of 1 day leads to a *ca.* 60 % increment in the Te/Mo molar ratio and triples that of V/Mo in the resulting precipitate. Regardless of the synthesis time, Te/Mo and especially V/Mo values in 110 °C precipitates are not even achieved with the longest synthesis times at 80 °C.

These changes in the chemical composition among solids precipitated by reflux at different temperatures and synthesis times (table 1) are reflected in relevant morphology variations. Thus, two differentiated morphologies are present in precursors with V/Mo molar ratio bellow 0.16: i) micrometer-scale rod-shaped crystals, and ii) amorphous-like conglomerate formed by aggregated nanometer-scale clusters. As a case in point, a FESEM micrography of the precipitate for 4 days at 80 ºC (sample L-4) is displayed in Figure 2. On the other hand, only amorphous aggregates are observed in precursors with V/Mo molar ratio ≥ 0.16, where crystalline rod-shaped particles are hardly found, as shown *eg.* in FESEM micrographs of M-4 and P-4 samples (Figure 2).

The study of the chemical composition by EDAX of selected areas in FESEM micrographs, reveals a common enrichment of vanadium in all amorphous aggregates (average V/Mo molar ratio of 0.17), regardless of the reflux temperature, compared with the crystalline rod-shaped structures where vanadium is absent or hardly present (average

V/Mo molar ratio of 0.05). With respect to the Te/Mo molar ratio, it remains equivalent between both morphologies, with variable values within the 0.16-0.21 range. Nevertheless, a marked tendency for higher Nb content is found in the V-rich amorphous particles (0.24 average Nb/Mo molar ratio) compared with the rod-shaped long crystals which are poor in vanadium (0.17 average Nb/Mo molar ratio).

3.2. Characterization of Catalysts

The actual samples used as catalysts for propane partial oxidation reaction, which will be discussed later, result from the thermal activation treatment (600 °C/2h in N_2 stream) of the precipitates by reflux. In contrast with the low crystallinity observed by XRD for the precursors (Figure 1), their thermal activation gives rise to the formation of well-defined crystalline phases (Figure 3). The distributions of solid phases, calculated by Rietveld refinement from the catalysts XRD patterns, are displayed in Table 1. The L-1A catalyst, derived from the lowest both reflux temperature and synthesis time, mainly contain crystalline phases type M_5O_{14} (45%) [JCPDS: 31-1437] and TeM_5O_{16} (18%) [JCPDS: 31-0874], as well as a significant amount of amorphous solid (38%). This catalyst presents no trace of $(TeO)_2M_{20}O_{56}$ structure [JCPDS: 18-582], the so-called M1 phase, directly related with the selective conversion of the alkane [10, 11, 16-29]. As increasing the time used to prepare the precursor at 80 °C reflux, the content in TeM_5O_{16} structure grows up and the M1 phase starts gradually emerging in the resulting catalysts (samples L-2A and L-4A), while M_5O_{14} and especially amorphous solids recede (Table 1). Moving the reflux temperature from 80 to 100 °C, at equivalent synthesis times, also enhances the content of M1 phase in the final activated catalysts, even more drastically than extending the synthesis time. Thus, the precursor precipitated for 1day reflux synthesis at 100 °C leads

to a final activated catalyst (sample M-1A) with M1 phase amount slightly above that for the catalyst derived from 4 times longer synthesis at 80 °C (sample L-1A). Something similar occurs with the 110 °C synthesis, where the catalyst derived from the shortest reflux time (sample P-1A) equals and doubles the M1 phase content of catalysts from 4 times longer synthesis at 100 and 80 °C, respectively. However, for the case of 110 °C precursor synthesis, the time-dependent effect on the M1 phase amount in the resulting activated catalyst (increments ≤ 5%) is not so strong than for 80 and 100 °C syntheses. On the other hand, no $Te_{0.33}MO_{3.33}$ (the so-called M2 phase: *M*= Mo, V, Nb) has been observed in these catalysts, regardless of the synthesis conditions. In this way, we must indicate that this phase is usually observed in Mo-V-Te-Nb-O catalysts prepared by coprecipitation [10, 16-18], but not frequent when the catalysts are hydrothermally prepared [16, 19-21].

Heat-treated samples of L- and M-series (i.e. samples prepared at 80 and 100ºC, respectively) are characterized by the presence of Raman bands at ca. 936, 860, 796, 459, 340 and 240 cm^{-1} with shoulders at 684 and 994 cm^{-1} (**Fig. S1**, in supplementary information). Bands at, 936, 860, and 684 cm^{-1} have been attributed to M_5O_{14} crystallites (with *M*= Mo, V, W) [35, 36]. The shoulder at ca. 990 cm^{-1} can be assigned to stretching vibrations of terminal Mo=O and V=O bonds [37]. In the case of P-series catalysts, especially that from 4 days precursor precipitation (P-4A), the Raman spectra show the main presence of bands at 872 and 478 cm^{-1} (also observed as minority ones in M-series catalysts) which have been related to M1 phase [38]. In this way, it has been proposed that in the case of M1 phase, the bands at 770–880 cm^{-1} appear in a typical regime of asymmetric cation–O–cation bridge stretching modes, while the low-frequency band (at *ca.* 470 cm^{-1}) appears in a typical regime of the symmetric one [38]. Although Raman spectra confirm the XRD results, still provide meaningless information about the nature

of non-crystalline phases. Anyway, the amorphous content is a minority in the case of catalysts mainly presenting M1 phase (i.e. P-4A).

Comparing the results from chemical composition analyses of the precursors and the distribution of phases in the catalysts, a direct relation is found between the incorporation of vanadium in the precursor and the formation of M1 phase upon thermal activation. Figure 4 displays a linear correlation between the percentage of M1 phase present in the catalysts and the V/Mo molar ratio in the corresponding precursor, with a limit apparently established from 0.16 V/Mo values. At this point, it should be reminded that V incorporation in the precursor (Table 1), favored for longer synthesis time and especially for higher reflux temperature, was preferentially observed (EDAX-FESEM) in the amorphous-like aggregates. Accordingly, the higher the V/Mo molar ratio in the precursor the higher the presence of amorphous-like conglomerate observed by FESEM, compared with the V-free rod-shaped crystals (Figure 2). A maximum is reached for the highest V/Mo values ≥ 0.16, where long crystals cannot be found by FESEM.

Although it is coherent the buffered growth of M1 phase in the catalysts derived from 110 °C precursors whose V/Mo molar ratios (within 0.16-0.17) are not gradually increasing, the correlation in Figure 4 does not explain the even small but significant increment of the cited active phase in these samples. Instead, XPS results of these catalysts from P-series (i.e. those derived from 110 °C synthesis) seem to shed some light on the issue (Table 2), since the synthesis time for the reflux synthesis at 110 °C shows to have an important effect on the electronic configuration of the elements near the surface of the resulting catalyst. The most relevant effect is observed for vanadium. Thus, a minority +4 oxidation state (16% V^{+4}) in the P-1 catalyst, derived from 1 day reflux precipitate, is drastically inverted as increasing the precursor synthesis time, to become the major oxidation state in the catalysts derived from 2 days and 4 days reflux precipitates, with

64% and 83% V^{+4}, respectively. Regarding the Te and Nb near surface in the catalysts derived from 110 °C reflux precipitates, they mainly appear as Te^{+4} and Nb^{+5}. Both elements undergo definitive stabilization in their respective electronic configurations near-surface of the catalyst from the 48h reflux synthesis (P-2A catalyst). Thus, the mixed-valence Te^{+4} and Te^{+6} present in the P-1A catalyst is completely reduced to Te^{+4} in the P-2A catalyst, while niobium as Nb^{5+} was only observed (Table 2).

In Table 2 are shown also some redox features determined for the catalysts derived from precursors prepared at 110 °C (P-series). Redox potentials were calculated from the corresponding bandgap energy, i.e. the energy needed to promote an electron from the valence band into the conduction band. The bandgap energies have been obtained from the diffuse reflectance UV-vis spectra of the catalyst, representing the Kubelka-Munk equation as a function of the UV-vis adsorption energy measured, and extrapolating to the intersection point with the "x" axis where the given function is zero (Figure 5) [10]. Thus, redox potentials determined for the catalysts derived from 110 °C precursors are lower as increasing the synthesis time of the precursor, *i.e.* the catalyst is more reduced, so that it has less tendency to be reduced and therefore less oxidant character. This trend is confirmed by the results from temperature-programmed reduction with H_2 (H_2-TPR) of the catalysts P-1, P-2 and P-4, which present increasing temperature for the maximum of reduction, i.e. 504, 514 and 527 ºC, respectively (Table 2, and Fig. S2 in supplementary information).

The lower vanadium oxidation state observed by XPS for the P-series solids (Table 2) as increasing the synthesis time of the precipitate is in good agreement with the redox potentials (Table 2, Fig. 5) and the results of H_2-TPR (Table 2, Fig. S2 in supplementary information).

On the other hand, higher reflux temperatures and longer synthesis times give rise to final catalysts with proportionally increased surface areas (Table 1). Although in general, the areas are low, it is quite significant the gradual increment as increasing either temperature or time for the precursor precipitation by reflux synthesis (Table 1). Thus, the catalyst surface area is doubled as extending the synthesis time from 1 day to 4 days to prepare the precursor at 110 °C (P-series). Accordingly, FESEM micrographs of these catalysts (Fig. 6) show the averaged crystal size is significantly reduced in the catalyst derived from the precursor prepared at 4 days (**P-4** catalyst), which confirms the reliability of the surface area results, at least in relative terms.

3.3. Catalytic tests for propane oxidation and ethane oxidative dehydrogenation

The catalytic properties of these materials have been studied for the selective oxidation of propane to acrylic acid and for the oxidative dehydrogenation (ODH) of ethane within the 340-440 °C temperature range.

For propane partial oxidation, acrylic acid, propylene, acetic acid and carbon oxides are the main oxidation products (sum ≥ 97 % of total products) (Table S1). Acrylic acid appears as the main reaction product at alkane conversions above 20%, in all cases. On the contrary, lower propane conversions favor the production of propylene, as corresponds to its primary product condition. Acetic acid and CO_x, products involving C-C bond breaks, are more favored as the alkane conversion increases [14-21, 24]. The main catalytic results for propane partial oxidation are summarized in Figure 7a, which comparatively displays propane conversion and yield of acrylic acid for the most representative catalysts. In general, enhancements of both catalytic activity (propane conversion) and yield of acrylic acid are observed as increasing the reflux temperature

and synthesis time employed to precipitate the catalyst precursor. In the case of the catalysts derived from 80 °C reflux precipitates (with minority active phase, M1) the catalytic activity observed is very low (< 10 %), while the catalysts from 110 °C reflux precipitates (with the richest M1 phase contents) show the highest propane conversions and acrylic acid yields. Thus, the improvement in the propane selective conversion into acrylic acid over catalysts prepared at increased temperature and time of the precursor reflux synthesis is consistent with the enrichment of M1 active phase in the catalysts. Nevertheless, either alkane conversion or acrylic acid yield appears not proportional to the M1 phase content in the catalysts. Indeed, the variation of propane conversion with M1 phase content displayed in Figure 7b shows no linear correlation. Instead, the correlation presents an asymptotic behavior, with M1 phase reaching a maximum limit around 70%. Especially characteristic is the strong enhancement of catalytic activity observed for the catalysts derived from 110 °C synthesis as extending the reflux time to 96h (4 days), which cannot be explained with the small increment of M1 phase around the asymptotic limit (Figure 7b).

However, the gradual increased specific area (up to > 100%) along with the progressive drop in the redox potential (up to *ca.*50%), as moving from 1 to 4 days precursor synthesis, do appear to properly correlate with the outcoming doubled conversion and yield for propane partial oxidation to acrylic acid.

In the case of ethane ODH, ethylene, carbon monoxide, and carbon dioxide were only observed as reaction products, with a carbon balance of *ca.* 100 %. The most representative results, related to ethane conversion and yield to ethylene, are summarized in Figure 8a. All catalysts presented a selectivity to ethylene higher than 95% at a conversion of ethane lower than 30%, which agrees with previous catalytic results on Mo-V-Te-Nb-O mixed oxides reported as catalysts prepared hydrothermally [10, 11, 22] or

by co-precipitation [38, 39]. The presence of crystalline phases such as M_5O_{14} or TeM_5O_{16} (*M*= Mo, V, Nb) has no influence in both ethylene formation and ethylene combustion [38]. On the other hand, a parallelism between the propane partial oxidation and the ethane ODH is also observed, in agreement with previous results [38, 39]. In this way, although the key role of the M1 phase in the activity and the selectivity during both propane and ethane partial oxidation is clear, again no linear proportionality is found between the amount of M1 phase in the catalyst and the alkane conversion. Thus, the variation of ethane conversion with the M1 phase content displayed in Figure 8b shows a similar asymptotic behavior than that for propane conversion (Figure 7b).

4. Conclusions

A new synthesis method, based in reflux precipitation, is presented for developing complex Mo-V-Te-Nb mixed oxide catalysts. From the study about the effect of temperature and time for the synthesis of the catalyst precursor by reflux precipitation, a direct correlation can be established between the vanadium incorporation into the reflux precipitate and the rise of the synthesis temperature. Vanadium appears selectively incorporated into amorphous-like aggregates, favoring their formation versus rod-shaped crystals as increasing the vanadium content in the reflux precipitate. The higher the V/Mo molar ratio in these precursors the larger the amount of M1 active phase in the resulting activated catalyst.

Although vanadium incorporation into the reflux precipitate is also induced with longer synthesis time, the access to certain V/Mo molar ratios appears strictly conditioned by the temperature of the reflux synthesis. Thus, synthesis temperatures higher than 100 °C are needed to obtain precursors with high enough V/Mo molar ratios leading to a major

formation of M1 active phase (> 60%) in the final catalysts. The largest amount of M1 active phase has been obtained for an optimum reflux temperature of 110 °C. Longer synthesis times at 110 °C give rise to smaller crystal sizes in the final catalysts (higher surface area) and lower redox potentials mainly due to the reduction of V^{+5} to V^{+4}, which together result in a significant improvement of the catalytic properties, especially for the propane selective oxidation into acrylic acid. The optimum results have been achieved with the P-4A catalyst (*i.e.* from a precursor synthesis carried out at 110 °C for 4 days), exceeding 75% selectivity to acrylic acid from 20% to 50 % propane conversion at 400ºC (Figure 9). For the first time, a competitive catalytic performance in propane selective oxidation to acrylic acid has been achieved with catalysts prepared employing the reflux method, thereby overcoming by far the shortfalls from our former pioneering work [29]. Thus, it is demonstrated by comparing with the best catalytic results obtained with Mo-V-Te-Nb mixed oxide catalysts from previously reported investigations using optimized hydrothermal- or slurry-synthesis methods, as shown in figure 9.

Accordingly, the optimum results for ethane ODH were achieved on the same P-4A catalyst, showing a selectivity to ethylene above 95 within the 20-50 range of ethane conversion at 400ºC. In both cases there is a parallelism between the amount and optimum physicochemical characteristics of the M1 phase and the yield to acrylic acid (from propane) or to ethylene (from ethane).

Acknowledgments

Authors gratefully acknowledge the funds from DGICYT by the project RTI2018-099668-B-C21, as well as the funds from *Comunidad de Madrid* by the project 2017-

T1/IND-6025 within the program "*Atracción y Retención de Talento Investigador"* of the V PRICIT.

References

[1] R.K. Grasselli, J.D. Burrington, D.J. Buttrey, P. DeSanto, C.G. Lugmair, A.F. Volpe, T. Weingand, Top. Catal., 23 (2003) 5-22.

[2] A. Chieregato, J.M. López Nieto, F. Cavani, Coord. Chem. Rev. 301-302 (2015) 3-23.

[3] J.C. Védrine, I. Fechete, Heterogeneous partial oxidation catalysis on metal oxides, Compt. Rend. Chim. 19 (2016) 1203-1225.

[4] J.M. Lopez Nieto, B. Solsona, Gas phase heterogeneous partial oxidation reactions, in: J.C. Vedrine (Ed.) Metal Oxides in Heterogeneous Catalysis, Elsevier, 2018, pp. 211-286.

[5] C. Sprung, G.S. Yablonsky, R. Schlögl, A. Trunschke, Catalysts, 8 (2018) 1-32.

[6] R.K. Grasselli,, Catal. Today 238 (2014) 10-27.

[7] J.M. López Nieto, B. Solsona, P. Concepcion, F. Ivars, A. Dejoz, M.I. Vazquez, Catal. Today, 157 (2010) 291-296.

[8] T. Ushikubo, H. Nakamura, Y. Koyasu, S. Wajiki, Method for producing an unsaturated carboxylic acid, US Patent 5,380,933,(1995), assigned to Mitsubushi Kasei Corporation, 1995.

[9] T. Ushikubo, K. Oshima, A. Kayou, M. Hatano, Stud. Surf. Sci. Catal. 112 (1997) 473-480.

[10] H. Tsuji, Y. Koyasu, J. Am. Chem. Soc. 124 (2002) 5608-5609.

[11] P. Botella, E. Garcia-Gonzalez, A. Dejoz, J.M. López Nieto, M.I. Vazquez, J. Gonzalez-Calbet, J. Catal. 225 (2004) 428-438.

[12] a) J.M. López Nieto, P. Botella, M.I. Vázquez, A. Dejoz, Method for the oxidative dehydrogenation of ethane, US Patent 7,319,179 B2 (2008); b) J.M. López Nieto, P. Botella, M.I. Vázquez, A. Dejoz, Method for the oxidative dehydrogenation of ethane, EP 1,479,438 A1 (2004), assigned to CSIC and UPV.

[13] J.L. Dubois, Catal. Today 99 (2005) 5-14.

[14] J.-L.P. Dubois, S. Gregory, J.M.M Millet, Propane-selective Oxidation to Acrylic Acid, in: M.V.d.V. Bert Sels (Ed.) Nanotechnology in Catalysis: Applications in the Chemical Industry, Energy Development, and Environment Protection, Wiley-VCH, 2017, pp. 503-535.

[15] A.M. Gaffney, O.M. Mason, Catal. Today 285 (2017) 159-165.

[16] P. Botella, E. García-González, J.M. López Nieto, J.M. González-Calbet, Solid State Sci. 7 (2005) 507-519.

[17] A. Celaya Sanfiz, T.W. Hansen, A. Sakthivel, A. Trunschke, R. Schlogl, A. Knoester, H.H. Brongersma, M.H. Looi, S.B.A. Hamid, J. Catal. 258 (2008) 35-43.

[18] T.T. Nguyen, B. Deniau, M. Baca, J.-M.M. Millet, Top. Catal. 59 (2016) 1496-1505.

[19] P. Botella, J.M. López Nieto, B. Solsona, A. Mifsud, F. Marquez, J. Catal. 209 (2002) 445-455.

[20] D. Vitry, Y. Morikawa, J.L. Dubois, W. Ueda, Appl. Catal. A: Gen 251 (2003) 411-424.

[21] A. Celaya Sanfiz, T.W. Hansen, F. Girgsdies, O. Timpe, E. Rodel, T. Ressler, A. Trunschke, R. Schlogl, Top. Catal. 50 (2008) 19-32.

[22] P. Beato, A. Blume, F. Girgsdies, R.E. Jentoft, R. Schlogl, O. Timpe, A. Trunschke, G. Weinberg, Q. Basher, F.A. Hamid, S.B.A. Hamid, E. Omar, L.M. Salim, Appl. Catal. A: Gen 307 (2006) 137-147.

[23] H. Hibst, F. Rosowski, G. Cox, Catal. Today 117 (2006) 234-241.

[24] A. Celaya Sanfiz, T.W. Hansen, D. Teschner, P. Schnoerch, F. Girgsdies, A. Trunschke, R. Schloegl, M.H. Looi, S.B.A. Hamid, J. Phys. Chem. C 114 (2010) 1912-1921.

[25] T.Y. Kardash, E.V. Lazareva, D.A. Svintsitskiy, A.V. Ishchenko, V.M. Bondareva, R.B. Neder, RSC Adv. 8 (2018) 35903-35916.

[26] P. Concepcion, S. Hernandez, J.M.Lopez Nieto, Appl. Catal. A: Gen 391 (2011) 92-101.

[27] M. Baca, J.M.M. Millet, Appl. Catal. A: Gen 279 (2005) 67-77.

[28] S. Lwin, W. Diao, C. Baroi, A.M. Gaffney, R.R. Fushimi, Catalysts, 7 (2017) 109.

[29] I. Ramli, P. Botella, F. Ivars, W. Pei Meng, S.M.M. Zawawi, H.A. Ahangar, S. Hernández, J.M.L. Nieto, J. Mol. Catal. A: Chem. 342-343 (2011) 50-57.

[30] P. Botella, A. Dejoz, J.M. López Nieto, P. Concepción, M.I. Vázquez, Appl. Catal. A: Gen 298 (2006) 16-23.

[31] H. D'Amour, R. Allmann, Z. Kristall. – Cryst. Mat. 1976, pp. 1.

[32] A. Leclaire, M.M. Borel, J. Chardon, B. Raveau, Mat. R. Bull. 30 (1995) 1075-1080.

[33] M.N. Corella-Ochoa, H.N. Miras, A. Kidd, D.-L. Long, L. Cronin, Chem. Commun. 47 (2011) 8799-8801.

[34] P. Botella, J.M. López Nieto, B. Solsona, Catal. Lett. 78 (2002) 383-387.

[35] G. Mestl, J. Raman Spect. 33 (2002) 333-347.

[36] M. Dieterle, G. Mestl, Phys. Chem. Chem. Phys. 4 (2002) 822-826.

[37] H. Knoezinger, H. Jeziorowski, J. Phys. Chem. 82 (1978) 2002-2005.

[38] B. Solsona, M.I. Vázquez, F. Ivars, A. Dejoz, P. Concepción, J.M. López Nieto, J. Catal. 252 (2007) 271-280.

[39] T.T. Nguyen, L. Burel, D.L. Nguyen, C. Pham-Huu, J.M.M. Millet, Appl. Catal. A: Gen. 433-434 (2012) 41-48.

Table 1. Synthesis conditions and chemical composition of the reflux precipitates and characteristics of catalysts.

Precursors					**Heat-treated samples (catalysts)**					
Sample	**Synthesis Conditions**	**Composition (ICP) [a]**			**Sample**	**Surface area**	**XRD results**			
		V/Mo	Te/Mo	Nb/Mo		(m^2 g^{-1})	M1 phase	M_5O_{14}	TeM_5O_{16}	**N.C.**
L-1	80°C/1 day	0.06	0.16	0.27	**L-1A**	0.1	< 1	45	18	38
L-2	80°C/2 days	0.08	0.20	0.23	**L-2A**	0.7	15	21	36	27
L-4	80°C/4 days	0.11	0.21	0.22	**L-4A**	1.4	32	20	39	9
M-1	100°C/1 day	0.13	0.23	0.27	**M-1A**	0.8	38	39	10	12
M-2	100°C/2 days	0.14	0.24	0.26	**M-2A**	2.5	55	24	8	13
M-4	100°C/4 days	0.16	0.26	0.28	**M-4A**	4.2	64	20	6	11
P-1	110°C/1 day	0.17	0.25	0.29	**P-1A**	2.0	64	18	4	14
P-2	110°C/2 days	0.16	0.25	0.27	**P-2A**	3.6	69	7	4	20
P-4	110°C/4 days	0.17	0.22	0.24	**P-4A**	4.6	73	3	5	19

a) Chemical composition of solid precursors measured by AES-ICP and expressed as molar ratio normalized with respect to Mo content. Only the significant digits without error are displayed (the measuring errors are ≤ 2%).

b) % of amorphous (N.C.) and crystalline phases: M_5O_{14} (*M*= Mo,V,Nb) [JCPDS: 31-1437]; TeM_5O_{16} (*M*= Mo,V,Nb) [JCPDS: 31-0874]; M1 phase: $(TeO)_2M_{20}O_{56}$ (*M*= Mo, V, Nb) [JCPDS: 18-582]; determined by *Rietveld* refinement from XRD patterns.

Table 2. XPS results and redox properties of catalysts derived from 110°C reflux precipitates (P-series) at different synthesis time.

Catalyst	XPS	M^{cat}/M_T (XPS) [b]			DRS-UV-vis		H_2-TPR
	Mo/V/Te/Nb [a]	V^{+4}	Te^{+4}	Nb^{+5}	E_{gap} (eV) [c]	P_{red} (1/eV) [d]	T_{red} (ºC) [e]
P-1A	1/0.09/0.38/0.29	0.16	0.73	0.67	1.1	0.91	504
P-2A	1/0.10/0.32/0.28	0.64	1	1	1.2	0.83	514
P-4A	1/0.09/0.36/0.26	0.83	1	1	1.9	0.53	527

a) Atomic ratio; **b)** M^{cat}/M_T, atomic ratio between the specific metal cation and the total amount of the element in all the oxidation states found: V(V) + V(IV), Te(VI) + Te(IV) and Nb(V); **c)** E_{gap}, Bandgap energy value taken as the intersection point with the x-axis (absorption energy) of the Kubelka-Munk function for a null value of the given function $[F(R\infty)h\nu]^{1/2}=0$. Kubelka-Munk equation represented as a function of the absorption energy measured in diffuse reflectance UV-vis spectrum in Fig. 5; **d)** P_{red}, redox potential, the inverse of the bandgap energy; **e)** T_{red}, the temperature at the maximum of the H_2-TPR curve.

Caption to figures

Fig. 1. Powder XRD patterns of precipitates obtained by reflux at temperatures of 80 (L-series), 100 (M-series) or 110 °C (P-series), and time of synthesis of 1, 2 or 4 days.

Fig. 2. FESEM images of reflux precipitates obtained by 4 days reflux synthesis at: 80 °C (sample L-4), 100 ºC (sample M-4) or 110 °C (sample P-4).

Fig. 3. XRD patterns of the catalysts (600 °C/N_2 treatment) derived from precursors precipitated by reflux at different temperatures (80 ºC, L-series; 100 ºC, M-series; 110 °C, P-series) and synthesis time (1, 2 or 4 days). Key to symbols for the majority phases present: (○) M_5O_{14} [JCPDS: 31-1437], (▲) TeM_5O_{16} [JCPDS: 31-0874], (*) $(TeO)_2M_{20}O_{56}$ [JCPDS: 18-582]; (*M*: Mo, V, Nb).

Fig. 4 Correlation between the V/Mo molar ratio measured by ICP-AES in reflux precipitates (catalyst precursors) and the content of $(TeO)_2M_{20}O_{56}$ structure (*M*= Mo, V, Nb) [JCPDS: 18-582], the so-called M1 phase, in the final activated catalysts (determined by *Rietveld* refinement of XRD patterns).

Fig. 5. Kubelka-Munk equation $[F(R\infty)hv]^{1/2}$ as a function of the absorption energy measured in the diffuse reflectance UV-vis spectra of the catalysts obtained from precursors precipitated by reflux at 110 °C for 1, 2 or 4 days (catalysts P-1A, P-2A, and P-4A, respectively).

Fig. **6** FESEM images of catalysts directly derived from thermal activation of precursors precipitated by reflux synthesis at 110 °C for 1 and 4 days: P-1A and P-4A catalysts, respectively. Comparatively, the L-4A catalyst is also included (derived from 80 ºC/4 days reflux precipitate).

Fig. 7. a) Propane conversion and yield of acrylic acid obtained during the partial oxidation of propane over catalysts derived from precipitates at different reflux temperatures and synthesis times. b) Variation of propane conversion with M1 phase content in the final catalyst (Table 1). Reaction conditions for propane partial oxidation: temperature= 380 °C; contact time, W/F= 814 $g_{cat}\ h^{-1}\ (mol_{C3H8})^{-1}$.

Fig. 8. a) Ethane conversion and yield of ethylene obtained during the ethane ODH over catalysts derived from precipitates at different reflux temperatures and synthesis

times. b) Variation of ethane conversion with M1 phase content in the final catalyst (Table 1). Reaction conditions for ethane ODH: temperature= 440 °C; contact time, W/F= 156 g_{cat} h^{-1} $(mol_{C3H8})^{-1}$.

Fig. 9. Variation of the selectivity to acrylic acid (AA) with the propane conversion for the best performing catalyst from the present work: (●) sample **P-4A**, derived from 110°C/4 days reflux synthesis. Comparatively, results for representative Mo-V-Te-Nb mixed oxide catalysts with the most optimized catalytic performance derived from previously reported investigations are included: (○) 80°C/14-days reflux synthesis [29], (□) 175°C/2-days hydrothermal synthesis [40], (■) 80°C/2-hours slurry synthesis using evaporation to dryness precipitation [40]. All catalysts were tested using the same reaction system.

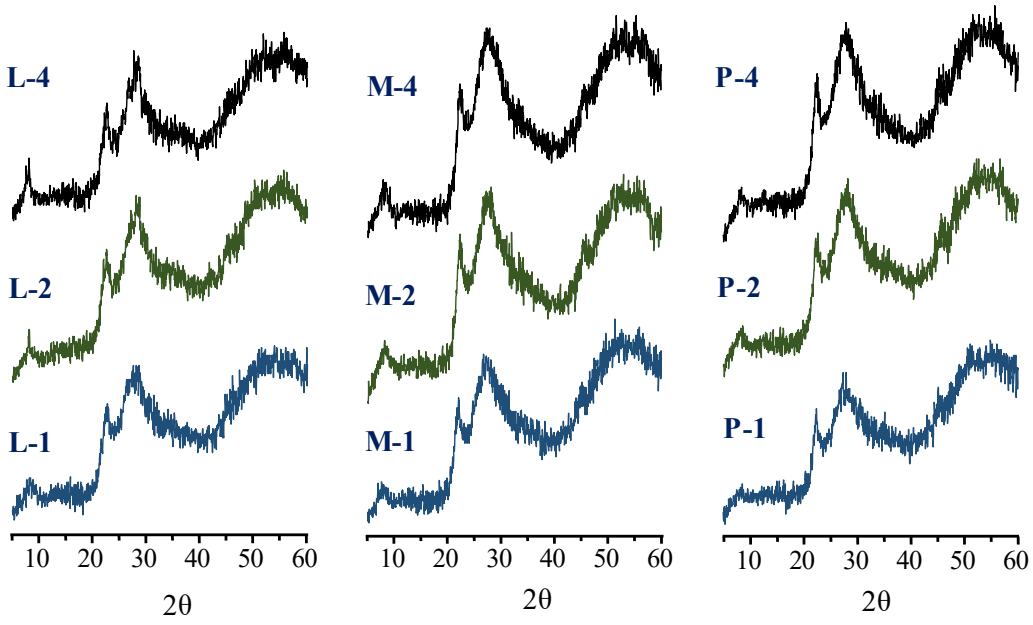
L-4
L-2
L-1
M-4
M-2
M-1
P-4
P-2
P-1
10 20 30 40 50 60
2θ
10 20 30 40 50 60
2θ
10 20 30 40 50 60
2θ

Fig. 1

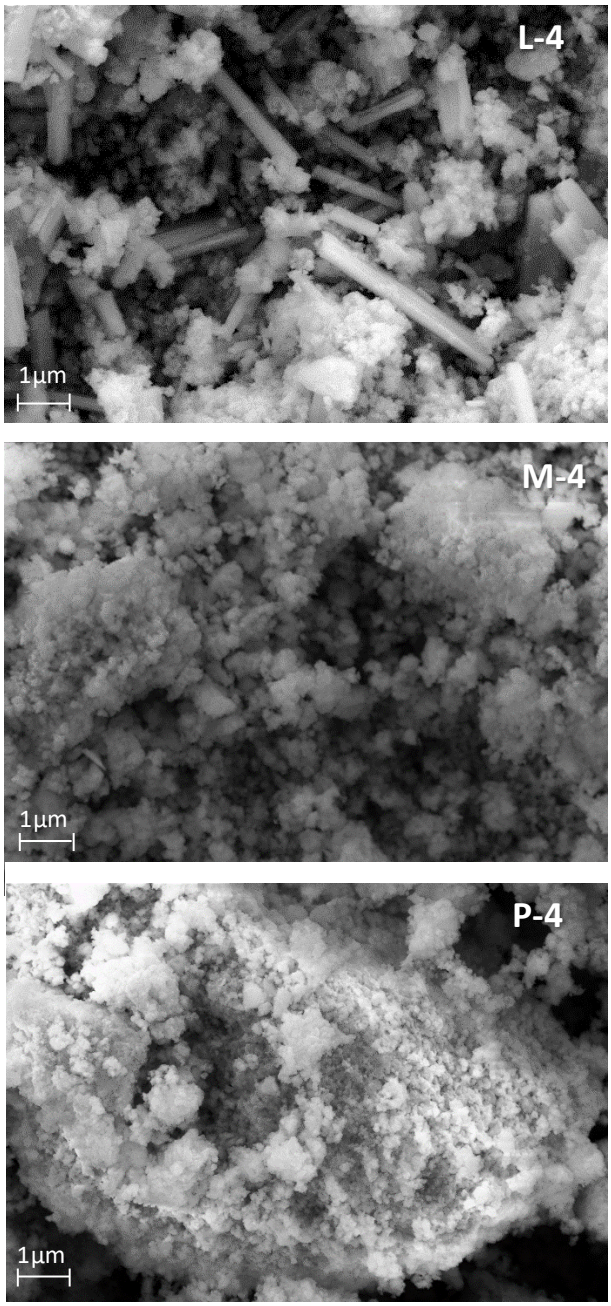

Fig. 2

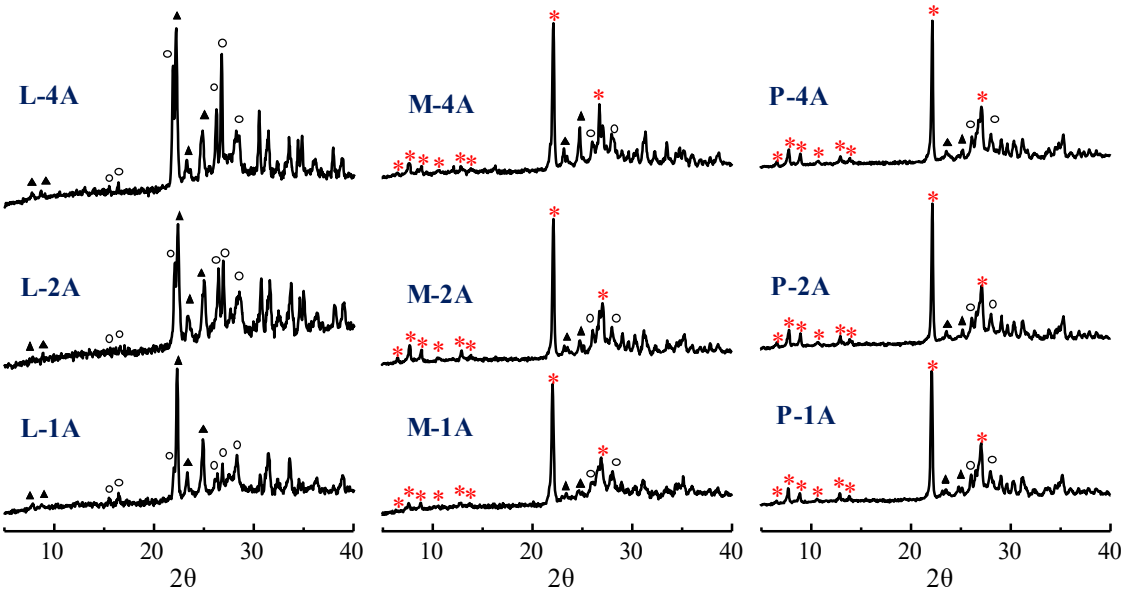
L-4A
M-4A
P-4A
L-2A
M-2A
P-2A
L-1A
M-1A
P-1A
10
20
30
40
2θ

Fig. 3

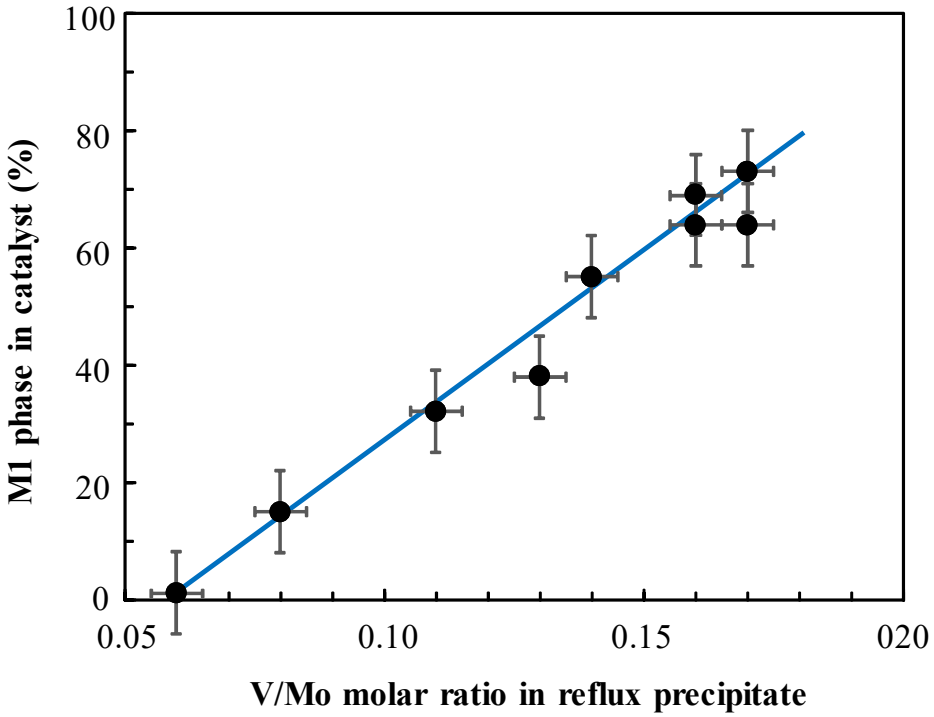
M1 phase in catalyst (%)
100
80
60
40
20
0
0.05
0.10
0.15
020
V/Mo molar ratio in reflux precipitate

Fig. 4

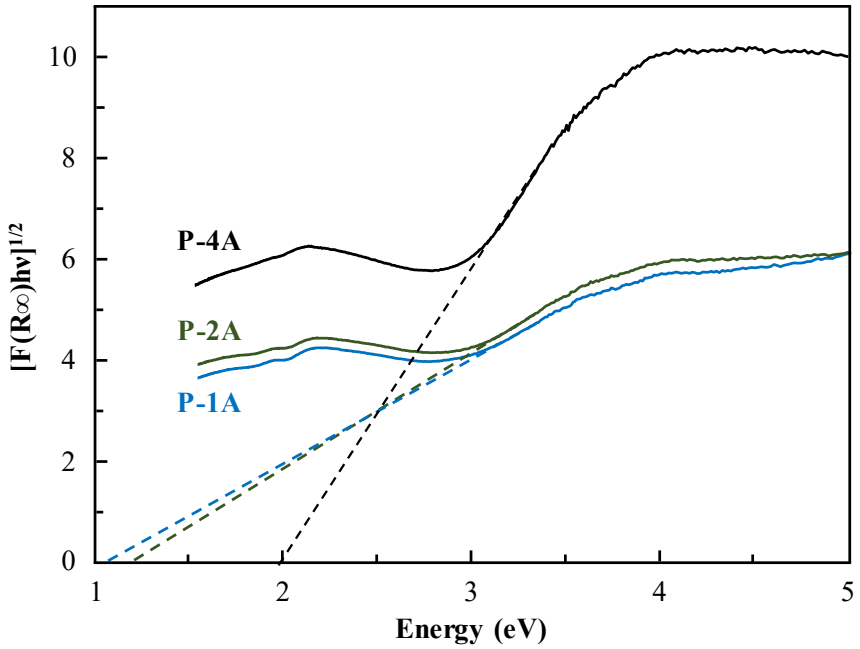

Fig. 5

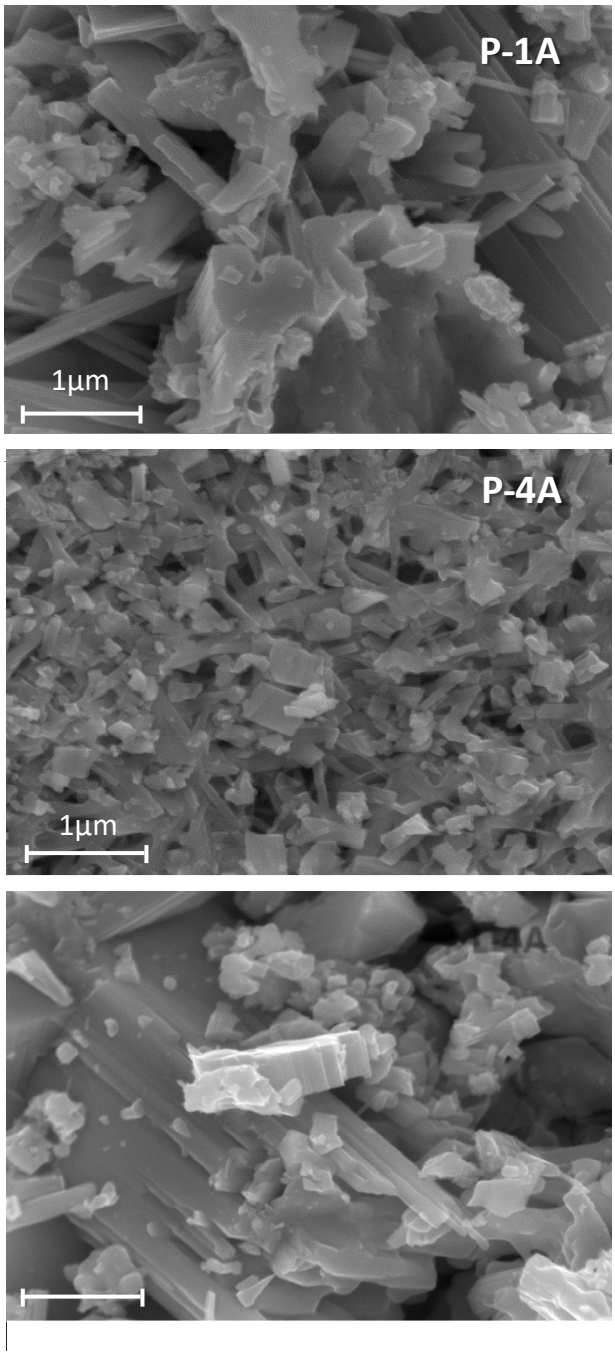

Fig. 6

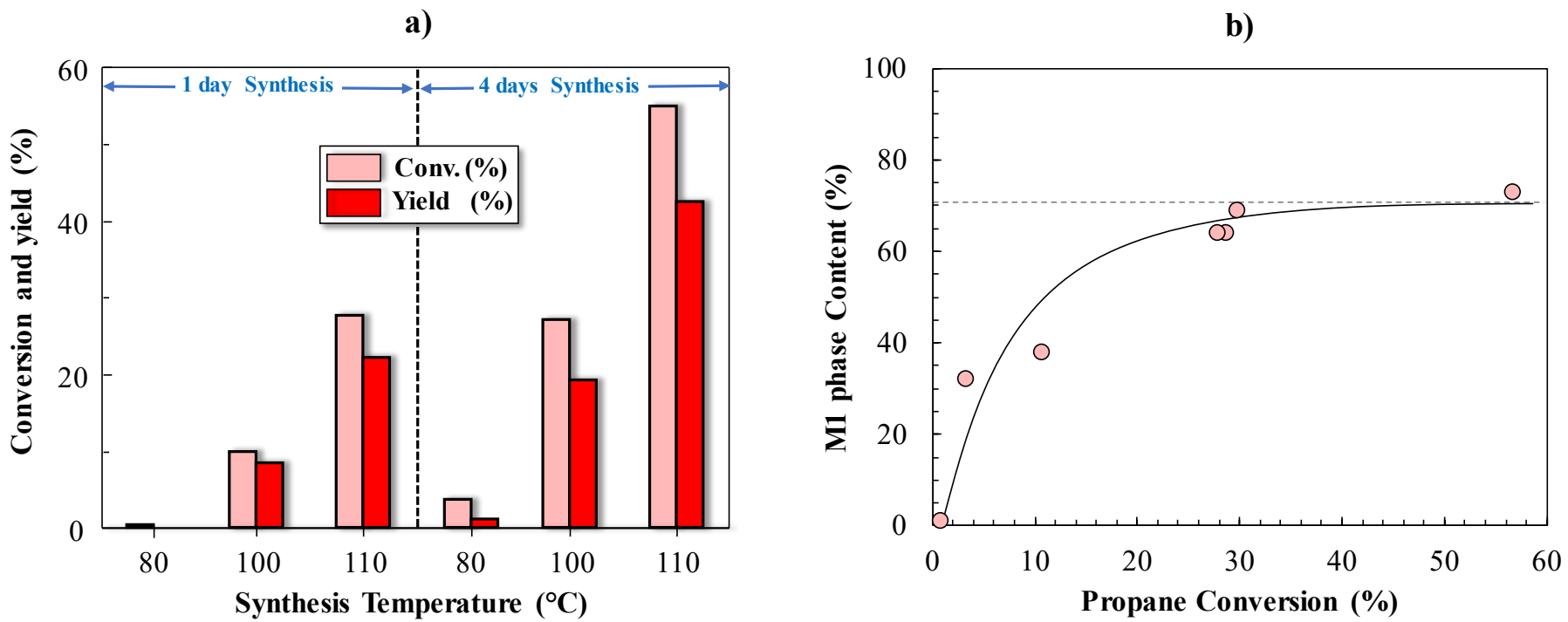
a)
b)
1 day Synthesis
4 days Synthesis
Conv. (%)
Yield (%)
Conversion and yield (%)
Synthesis Temperature (°C)
80
100
110
80
100
110
0
20
40
60
M1 phase Content (%)
Propane Conversion (%)
0
10
20
30
40
50
60
80
100

Fig. 7

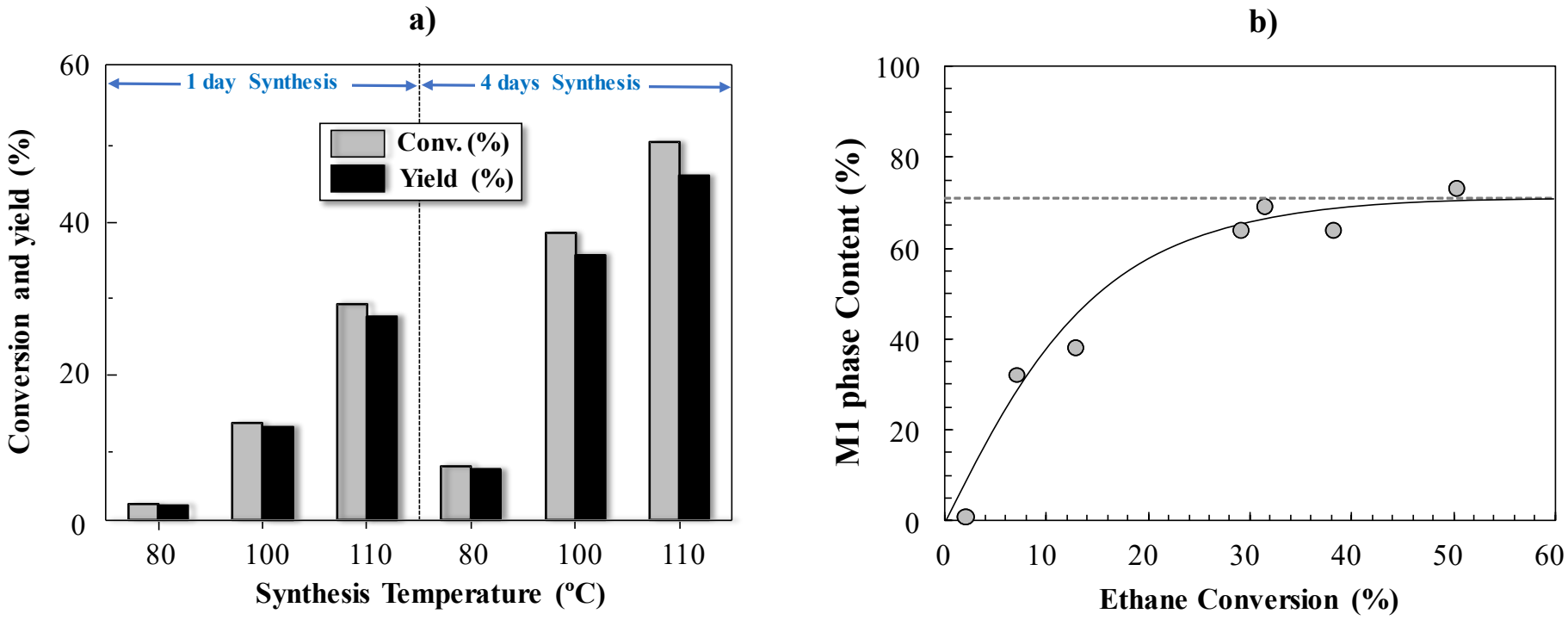
a)
1 day Synthesis
4 days Synthesis
Conv. (%)
Yield (%)
Conversion and yield (%)
0
20
40
60
80
100
110
80
100
110
Synthesis Temperature (ºC)
b)
M1 phase Content (%)
0
20
40
60
80
100
0
10
20
30
40
50
60
Ethane Conversion (%)

Fig. 8

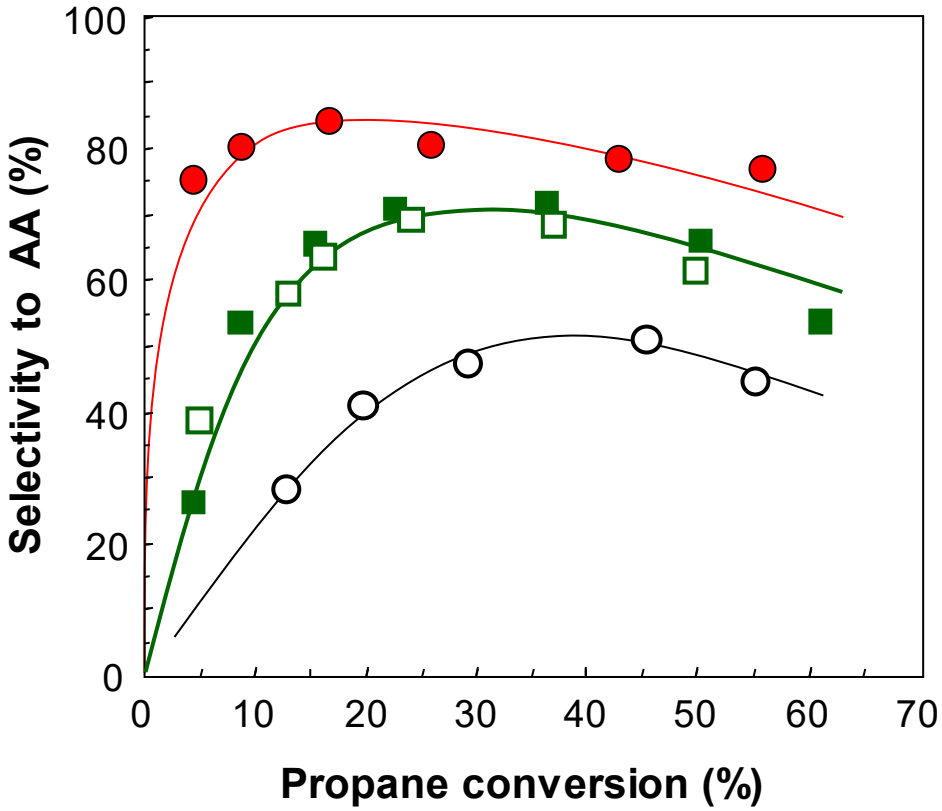
Selectivity to AA (%)
Propane conversion (%)
0
20
40
60
80
100
0
10
20
30
40
50
60
70

Fig. 9